Annales Geophysicae (2002) 20: 937–945 © European Geophysical Society 2002

Annales Geophysicae

Real-time forecasting of ICME shock arrivals at L1 during the "April Fool's Day" epoch: 28 March – 21 April 2001

W. Sun[1], M. Dryer[2,3], C. D. Fry[2], C. S. Deehr[1], Z. Smith[3], S.-I. Akasofu[4], M. D. Kartalev[5], and K. G. Grigorov[5]

[1]Geophysical Institute, University of Alaska Fairbanks, Fairbanks, Alaska, USA
[2]Exploration Physics International, Inc., Milford, New Hampshire, USA
[3]NOAA Space Environment Center, Boulder, Colorado, USA
[4]International Arctic Research Center, University of Alaska Fairbanks, Fairbanks, Alaska, USA
[5]Institute of Mechanics, Bulgarian Academy of Sciences, 1113 Sofia, Bulgaria

Received: 1 October 2001 – Revised: 31 January 2002 – Accepted: 18 February 2002

Abstract. The Sun was extremely active during the "April Fool's Day" epoch of 2001. We chose this period between a solar flare on 28 March 2001 to a final shock arrival at Earth on 21 April 2001. The activity consisted of two presumed helmet-streamer blowouts, seven M-class flares, and nine X-class flares, the last of which was behind the west limb. We have been experimenting since February 1997 with real-time, end-to-end forecasting of interplanetary coronal mass ejection (ICME) shock arrival times. Since August 1998, these forecasts have been distributed in real-time by e-mail to a list of interested scientists and operational USAF and NOAA forecasters. They are made using three different solar wind models. We describe here the solar events observed during the April Fool's 2001 epoch, along with the predicted and actual shock arrival times, and the *ex post facto* correction to the real-time coronal shock speed observations. It appears that the initial estimates of coronal shock speeds from Type II radio burst observations and coronal mass ejections were too high by as much as 30%. We conclude that a 3-dimensional coronal density model should be developed for application to observations of solar flares and their Type II radio burst observations.

Key words. Interplanetary physics (flare and stream dynamics; interplanetary shocks) – Magnetosheric physics (storms and substorms)

1 Introduction

An essential space weather objective is the need to understand and to predict the consequences at Earth of any solar activity after its evolution through the interplanetary medium. An obvious starting point is the reliable prediction of a solar flare-generated shock wave at Earth. We have reported our real-time forecasting experience, complete with statistics (metrics and forecasting skills) for several models (Smith et al., 2000; Fry et al., 2001; Dryer et al., 2002). The latter paper described the real-time and *ex post facto* modeling of ten flare-generated shocks during the "Bastille Day" epoch (7–15 July 2000). Another period of nearly daily solar activity took place the following year from 28 March 2001 to 21 April 2001 including the latter flare's shock arrival at Earth. We have, therefore, called the period the "April Fool's Day" epoch because of the large solar flares and several major geomagnetic storms evident in the large excursions of the geomagnetic field disturbance index, D_{st}.

The major objective of this paper will be similar to that described in the Bastille Day paper (Dryer et al., 2001) with two additional objectives. The forecasting skill of the Hakamada-Akasofu-Fry Version 2 (HAFv2.0) model was discussed in detail by Fry et al. (2001). The second objective will be to test the application of a real-time curve fitting and MHD shock analysis to ACE satellite observations of the solar wind at L1. The third objective will be to address the question: what is the accuracy level of the reported coronal shock speeds that are based on a spherically symmetric coronal density model?

We describe in Sect. 2 the solar flares, the real-time operationally available solar observations that are input to the HAFv2 model, and the ACE real-time solar wind and interplanetary magnetic field (IMF) data for the April Fool's Day epoch. Section 3 contains a description of the relationship between the shock arrivals tabulated in Sect. 2 and the disturbance geomagnetic field index, D_{st}. The results of the real-time predictions of plasma and IMF time series, as well as ecliptic plane plots of the shock-disturbed IMF are given in Sect. 4. The coronal shock speed (V_s) is modified via an iterative procedure to improve the predicted shock arrival time in Sect. 5. We will make some concluding remarks and suggestions in Sect. 6.

Correspondence to: W. Sun (sun@jupiter.gi.alaska.edu)

Table 1. Flares and shocks during the "April Fool's Day" epoch

Event No.	Fearless Forecast No.	Time from Last Event (Hrs)	Date DDMMYY	Start Time metric Type II (UT)	Coronal Shock Speed, Vs km/sec	Location	FLARE Classif. X-ray/Opt.	Piston-Driving Time, Tau HHMM	Active Region (AR)	SOHO/ LASCO Vcme POS, km/sec	Interplanetary Shocks at L1 (1) M. Dryer ACE or SOHO MDD	(1) HHMM	(2) D. Berdichevsky ACE ** MDD	(2) HHMM	(3) M. Kartalev (MHD)ACE *** MDD	(3) HHMM
1	255*	20	28/03/01	12:40	1000*	N18E02	M4.3/SF	04:00	9393	H: 530	330	21:50	330	21:50	330-SS	21:52
2	256	22	29/03/01	10:04	1300	N16W12	X1.7/1N	02:00	9393	H: 991	331	00:30	331	00:30	331	00:21
3	257*	30	30/03/01	15:59	1850	S10W90*	Blowout?	01:00	Helmet St	none						
4	258*	0.3	30/03/01	16:20	1600	S10E115*	Blowout?	01:00	Helmet St	3-part						
5	259	19	31/03/01	11:32	1200	N16W34	M2.1/SF	01:00	9393	none					403	15:38
6	260*A.Fool's	25	01/04/01	12:17	2000	S20E110*	M5.5/occl.	04:30	No Opt.	H:						
7	261*	7.5	01/04/01	19:49	800*	N17W57	M4.0/1F	01:00	9393	H:						
8	262	7	02/04/01	11:10	1542	N17W63	X1.1/1B	01:45	9393	none						
9	263*	11	02/04/01	21:52	2300	N21W67	X20/cldy	01:30	9393	H: 2291	404	14:21	404	14:22	404	14:21
10	264	6	03/04/01	03:57	1190	S22E72	X1.0/1N	02:45	9415	P-H 1190						
11	265*	61	05/04/01	17:25	1100*	S24E50	M5.1/2N	02:30	9415	H: 1046	407	17:00	407	16:55	407	16:59
12	266*	26	06/04/01	19:21	2000*	S21E31	X5.6/cldy	00:30	9415	H: 1103	408	10:30	408	10:33	408	10:33
13	267	72	09/04/01	15:27	800	S21W04	M7.9/2B	02:00	9415	H: 1086	411	13:11	411	13:14	411	13:11
14	268	14	10/04/01	05:13	2100	S23W09	X2.3/3B	03:00	9415	H: 1678	411	15:20	411	15:28	No Shock	
15	269	28	11/04/01	13:17	1231	S22W27	M2.3/1F	01:30	9415	H: 750	413	07:05	413	07:10	No Shock	
16	270*Gagarin	21	12/04/01	10:18	920	S22W40	X2.0/cldy	02:00	9415	H: 912	414	01:20	414	01:26	Tangential	Disc.
17	271 Easter	76	15/04/01	13:47	2773	S20W85	X14.4/2B	02:00	9415	1110	418	00:00	418	00:00	418	00:04
18	272*	61	18/04/01	02:17	2500*	S20W120	C2.2/occl.	03:00	9415	none	421	15:00	421	15:05	421	15:05

* = Indicates that a full set of input conditions was not available; hence, the asterisked parameter was assumed on a heuristic basis.
* = from Daniel Berdichevsky, (as of 21 April)
** = from Monio Kartalev's MHD analysis of ACE data, (as of 25 April)
Helmet St = Lack of X-ray flare signature suggests that a helmet streamer was destablized to create a 3-part CME in Event No. 4.
none = CME information was not available at the time of the fearless forecast for Event Numbers 3, 5, 8, and 18.
P-H = Partial Halo CME.
H: = Halo CME with the Plane-of-Sky (POS) speed as shown; otherwise they were not known. Position angles of this value are not shown.
occl. = Backside event was occulted by the Sun's limb. Thus, no H-alpha optical classification is meaningful.
cldy = Real-time reporting optical observatories were clouded over at the start and peak of the X-ray flare observations. We used the location assigned by NOAA/SWO.
Blowout? = Suspected helmet streamer destabilization (blowout) due to flux emergence or other unknown physical process.
No Opt. = No H-alpha optical observations were available due to an east Limb occultation of an as yet unnumbered Active Region.
SS = Slow Shock

2 Solar flares and observed interplanetary shocks at L1 during the April Fool's Day epoch

Table 1 shows 18 consecutive solar flares and helmet stream blowouts that were identified by Type II radio bursts and/or coronal mass ejections (CME), so they could be used in real-time forecasting of shock arrival times (SAT) at L1. The first column lists the consecutive event numbers which will be useful later in identifying the global ecliptic plane simulations. The second column, labeled "Fearless Forecast Number", is a running record of the real-time procedure that started in February 1997 with the events described by Smith et al. (2000). The third column is the approximate time in hours that elapsed since the previous event using the metric Type II start times. The fourth and fifth columns show these "start" times and the event locations. The metric Type II coronal shock speeds are listed in the sixth column followed by the location and classifications (X-ray and H-alpha) in the next two columns. The piston driving time, tau (τ), in the ninth column is the time at which the shock is assumed

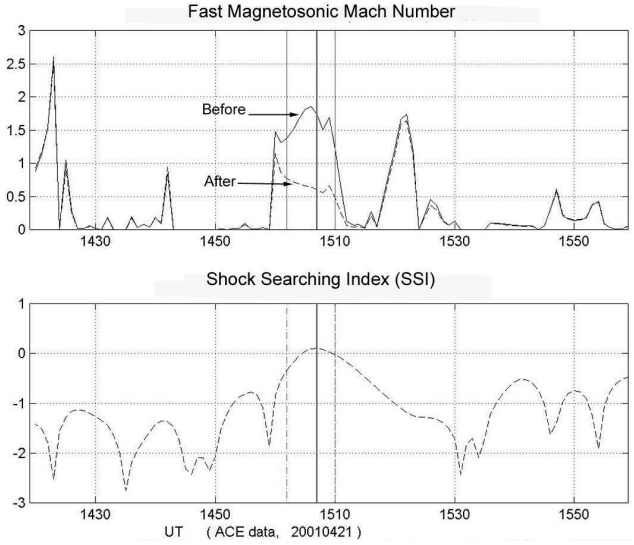

Fig. 1. (Upper panel) Determination of the fast magnetosonic Mach number for the actual Ll shock arrival for Event 18 (see Table 1). (Lower panel) The shock searching index (Eq. (1), applied to ACE, real-time data for dynamic pressure). The solid vertical line indicates the suggested center of the shock at 15:07 UT on 21 April 2001. The two dashed vertical lines indicate the shock thickness during the elapsed time: 15:02$< t <$15:10 UT. The local shock speed was 345 km/s in the direction of the shock normal vector: (-0.78, -0.1, -0.62) in GSE coordinates. The maximum jump of the fast magnetosonic Mach number from 1.72 upstream to 0.60 downstream (computed using the solar wind velocity relative to the shock) is at 15:07 UT. Thus, the estimated shock thickness was on the order of 2×10^5 km. Other derived shock parameters: sonic Mach number $\sim$2.4; Alfvén Mach number $\sim$2.5.

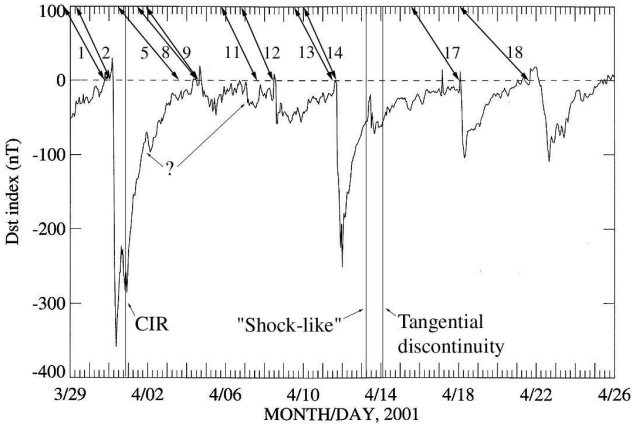

Fig. 2. Temporal profile of the D_{st} index (WDC, Kyoto) for the "April Fool's Day" Epoch. The double arrows on the top indicate the linkage between the solar flare time and the SSC time.

to be driven at constant speed (V_s); the soft X-ray duration time is used as a proxy to provide this estimate. The NOAA-assigned solar active region number, within which the flare took place, is provided in the tenth column. The last six columns give the shock arrival times at L1 as independently estimated by one of the authors, (MD), a NASA/ISTP scientist (D. Berdichevsky, private communication, 2001), and a rigorous real-time data curve fitting and MHD shock analysis by two of the present authors (MDK and KGG; see, also, Kartalev et al., 2002). Additional clarification of various notations is provided by the footnotes to Table 1.

An example of one of the outputs from the rigorous shock detection algorithm is shown in Fig. 1 for the shock from Event 18 on 21 April 2001 at 15:07 UT. This result before and after the shock is found from a curve-fitting procedure for each of the ACE plasma and IMF parameters. The density, n, temperature, T, and radial velocity (only), V_{sw}, as well as the three components of the IMF vector are all used. The derived dynamic pressure is also used as a check in the same form of a "shock searching index", SSI, as used by the HAF v.2 simulation model. Here, however, actual observations are used for this index in the form of the following equation (Dryer et al., 2001):

$$\mathrm{SSI} = \log 10 \left[DP(t+1) - DP(t) \right] / DP(t) \,, \qquad (1)$$

where DP is the dynamic pressure. The lower plot in Fig. 1 shows that SSI does in fact have a maximum where the upstream fast magnetosonic Mach number has its maximum ($>$1.0) simultaneously with a downstream value that is $<$ 1.0. This result was obtained for the events listed as SATs in the last two columns of Table 1. Note, however, that "No Shock" is listed for Events 14 and 15, in disagreement with the preliminary "eyeball" estimates of the other two individuals. Event 16 is listed as a tangential discontinuity, again in disagreement. Otherwise, all of the other shock identifications are in agreement. Event 5, on the other hand, was identified as having a shock arrival (as discussed further in Sects. 3 and 4) by the more rigorous method but not by the "eyeball" method.

3 Geoeffectiveness of interplanetary shocks

In general, the dayside magnetopause of the Earth is compressed by interplanetary shocks to produce the Chapman-Ferraro current (Chapman and Ferraro, 1931) leading to a sudden increase of the north-south component of the geomagnetic field, the so-called "storm sudden commencement" (SSC). Meanwhile, the ring current belt at the equatorial plane of the magnetosphere will be enhanced if the IMF turns southward. The decrease of the north-south component of the geomagnetic field generated by the enhancement of the ring current belt indicates the occurrence of a geomagnetic storm (Gonzalez et al., 1994). Figure 2 shows the D_{st} profiles for the April Fool's Day epoch. The double arrows on the top of Fig. 2 indicate the linkage between the solar flare time and the SSC time in the D_{st} index.

Ten of the eleven observed shocks in Table 1 caused SSCs in the D_{st} index. Event 2 was generated by an X1.7 flare that

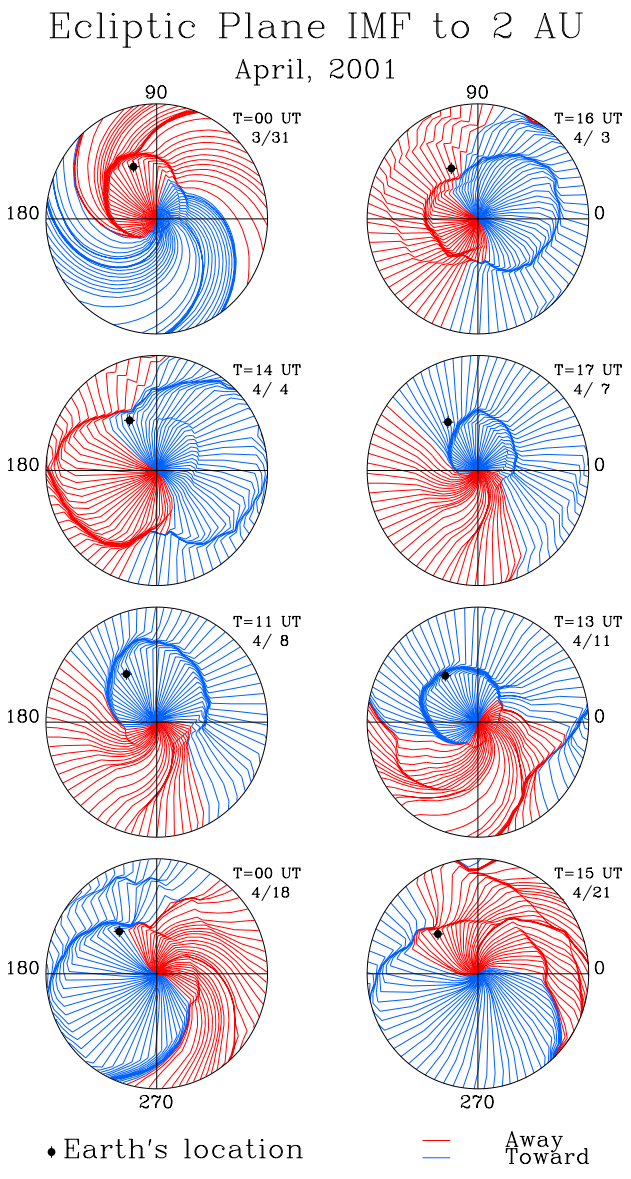

Fig. 3. Real-time simulation of the IMF's shock-induced distortions in the ecliptic plane out to 2 AU. The dates and times are chosen as close as possible to the eight actual shock arrivals listed in the last column of Table 1. Red curves represent the "away" IMF polarity; blue curves, "toward" polarity. Note that most simulated shocks are not predicted precisely at the actual times; see also Fig. 4.

overwhelmed the contribution from Event 1. The interplanetary shock at L1 caused by this flare is clearly identified with an intense SSC that occurred at 04:00 UT on 31 March 2001. The following development of the ring current belt was related to the southward turning of the IMF vector and formed one of the most intense geomagnetic storms in the last decade (minimum D_{st} was -358 nT). Event 5 produced no observable effect in the D_{st}. The effects of Events 8 and 9 and 13 and 14 could not be separated in the D_{st} record. The three intense geomagnetic storms at 16:00 UT on 11 April 2001, 02:00 UT on 18 April 2001 and 03:00 UT on 22 April 2001, were caused by the interplanetary shocks generated by events 13, 17 and 18, respectively. In particular, Event 18 at W120° could produce an intense geomagnetic storm despite the fact that the flare site was unseen from Earth. This result suggests that the lower coronal part of the expanding shock was very likely the source of the GeV-level particle energization that had a direct line-of-sight access to Earth. We might further suggest that the flaring (reconnection) process provided the particle "seed" population for the strong lower coronal part of the shock. This same shock, as will be seen below, was a "hemisphere buster" in the sense that it was sufficiently powerful to reach Earth from behind the solar limb.

4 Real-time forecast results

Figure 3 shows an ecliptic plane presentation out to 2 AU of the IMF during the "April Fool's Day" epoch. The red lines are field lines directed away from the Sun and the blue represents field lines directed toward the Sun. Note that the Earth's location is indicated by the black dot. The times for each circular panel (left to right and moving downward) were chosen to correspond as closely as possible to the actual SATs, as given by the eight rigorous shock detection times (labeled "M. Kartalev") in Table 1. Thus, the events identified with each ICME can be directly associated in Table 1.

Note, however, that the predicted shocks do not always impact the Earth's magnetosphere at the actual SATs. This fact can also be seen by referring to Fig. 4, which shows the time series of the solar wind speed, density, dynamic pressure, and SSI (see Eq. 1). Similarly, Fig. 5 shows a repetition of the speed and density plus the total IMF magnitude, its theta (θ) angle in GSM coordinates, and the phi (ϕ) angle sector orientation in GSE coordinates.

The blue lines in both Figs. 4 and 5 indicate the HAFv.2 simulation without any solar activity, i.e. only the source surface maps of Br and V for Carrington Rotations 1974 and 1975 are input to the heliospheric simulation. The red lines are the simulated responses when the solar flare and helmet streamer blowouts are mimicked by kinetic energy inputs, as described by Fry et al. (2001) on the basis of available real-time observational inputs. The black curves are the real-time solar wind plasma and IMF data provided by ACE/SWEPAM/MAG. Note that several plasma data dropouts (seen in the speed) on 3 April and 15 April 2001 occurred as a result of energetic flare proton bombardment and should be ignored. We feel it inappropriate to show Level 2 data since this paper is directed toward real-time prediction and analysis.

The reader can see immediately that the delta Ts (predicted minus actual) are often on the order of 10–12 h. These values are representative of our previous metric studies by Smith et al. (2000), Fry et al. (2001) and Dryer et al. (2001). An obvious question, therefore, is: to which of the observables is the SAT most sensitive? We believe that the initial coronal shock speed is representative of the total energy injected by the flare into the pre-existing solar wind (Dryer, 1994). Thus,

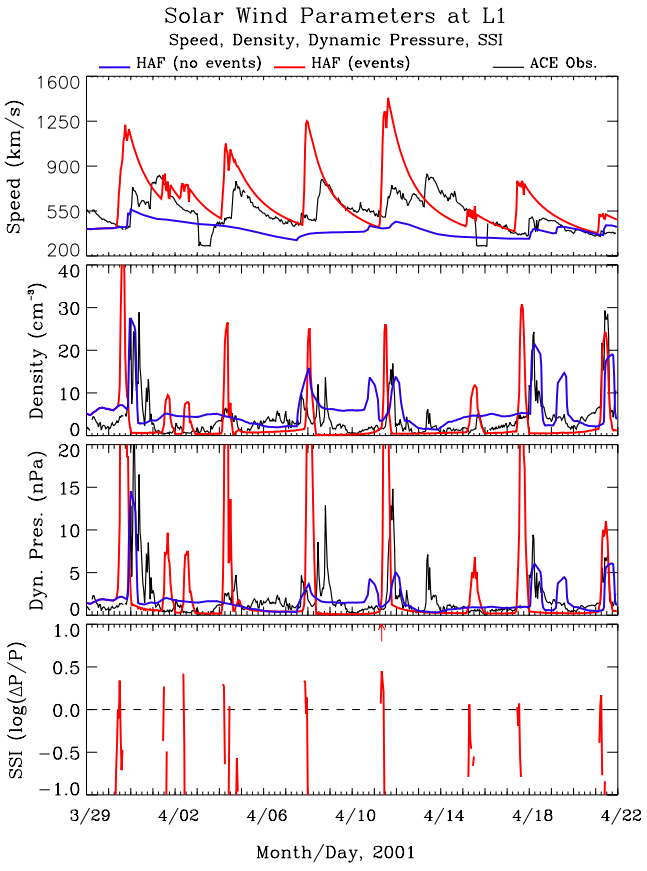

Fig. 4. Time series of real-time predicted (red curves) solar wind speed, density, and dynamic pressure and their comparison with the actual real-time ACE data (black curves) at LI during the "April Fool's Day" epoch. The blue curves represent the HAFv.2 simulation based only the Event-free solar source surface map inputs of Br and Vr at 2.5 R_S. The bottom panel shows the hourly-computed shock searching index, SSI (Eq. 1), used by the HAFv.2 model for the shock prediction procedure.

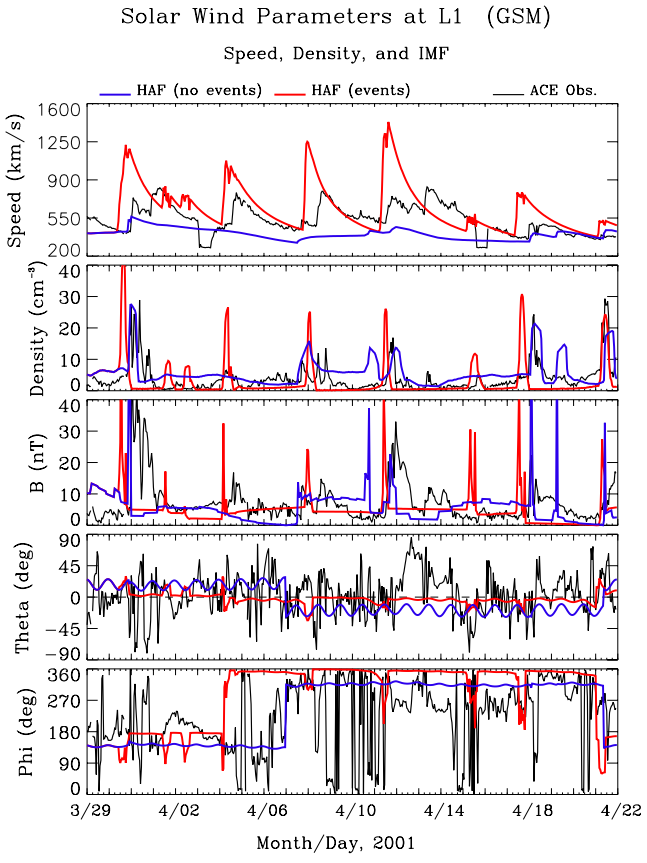

Fig. 5. Time series of real-time predicted solar wind plasma and magnetic field parameters at L1 and their comparison with the actual ACE real-time data, as in Fig. 4. Speed and density are repeated from Fig. 4. B is the total IMF magnitude; theta (θ) is the IMF's polar angle in GSM coordinate system and phi (ϕ) is the IMF's azimuthal angle in GSE coordinate system.

Table 2. Relative factors used to improve real-time simulated shock arrival times via iteration to reduce ΔTs (Predicted minus actual shock arrival times)

No	FFNo	V_s (km/s)	V_{si} (km/s)	FACTOR
1	255	1000	700	-0.30
2	256	1300	850	-0.35
3	257	1850	1200	-0.35
4	258	1600	1000	-0.38
5	259	1200	550	-0.54
6	260	2000	1500	-0.25
7	261	800	700	-0.13
8	262	1542	1400	-0.09
9	263	2300	1550	-0.33
10	264	1190	1190	0.0
11	265	1100	1500	0.36
12	266	2000	1350	-0.33
13	267	800	1150	0.4
14	268	2100	1500	-0.29
15	269	1231	1231	0.0
16	270	920	1200	0.30
17	271	2773	1700	-0.37
18	272	2500	1700	-0.32

the other observables (flare duration, size of the CME, etc.) should reflect this energy release. As a first hypothesis, therefore, we ask a related question: by how large a factor must we multiply the real-time Type II drift speeds to force the simulation to provide delta T's as close to zero as possible? We have attempted to answer this question in Sect. 5.

5 *Ex Post Facto* iterated "forecast" results

Figures 6, 7, and 8 are identical to the previous three figures with an important difference. In these figures, the initial coronal shock speeds, V_s, were iterated until a reasonably close SAT was achieved, i.e. until the ΔT close to zero was found. The relative factors, $(V_{si} - V_s)/V_s$, where V_{si} is the iterated speed used to improve the SAT via this empirical approach, are listed in Table 2. Note that two values of V_s were not changed; three were increased by approximately 30% and thirteen were decreased by approximately 35%. The results are then shown in Figs. 6, 7, and 8.

Several specific cases may be followed in the upper panel of Fig. 7 for the solar wind speed. Note that the combined result of Events 1 and 2 produce the shock at ~00:00 UT, 31 March 2001. We will return below to this shock because of the interest in its association with the major geomagnetic storm shown in Fig. 2. Referring to other events, it is seen that the sudden increase in the non-event curve (blue) on 30

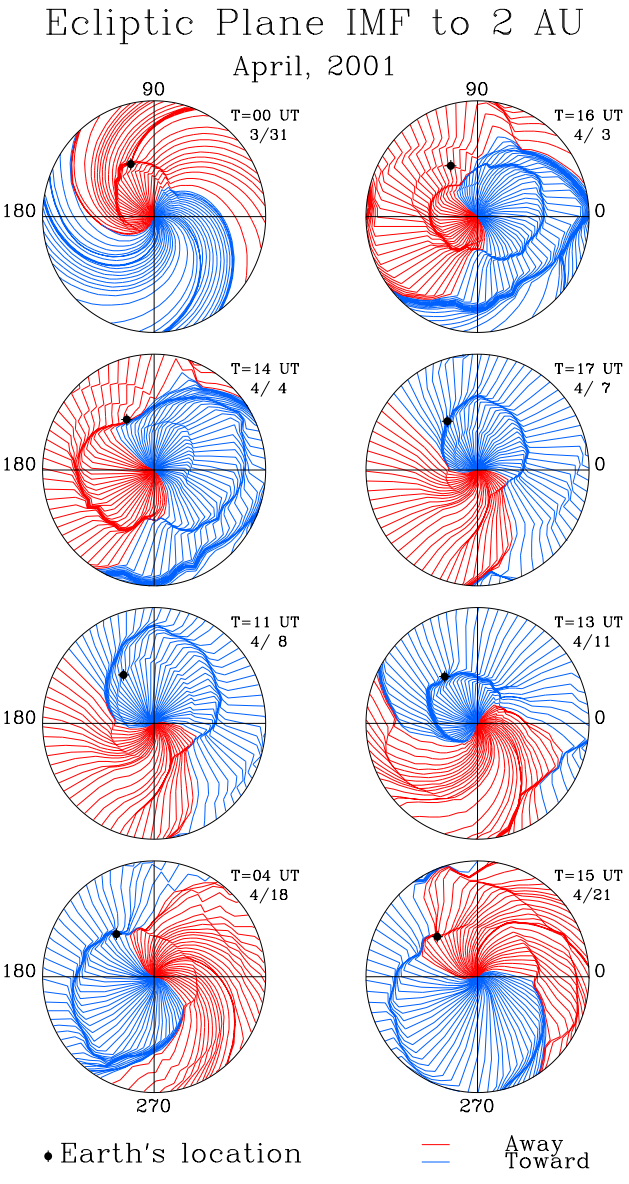

Fig. 6. Iterated *ex post facto* simulation of the IMF/shock distortions in the ecliptic plane out to 2 AU. These results were obtained after the real-time reported coronal shock speeds, V_s, were adjusted (see Table 2) to achieve improved shock arrival times, as given in the upper-right corner of each circular panel. Red and blue curves represent the "away" and "toward" IMF polarities, as shown in Fig. 3.

March, represents an early prediction of a CIR shock that actually arrived late on 31 March.

Moving on, Event 3 was predicted to arrive, but was not observed. Events 4 and 7 were predicted not to arrive and were not observed. Event 5 represents the actual shock arrival on 3 April following the recovery of ACE/SWEPAM Level 2 data that are not shown here; only the dropout in the real-time data is shown here.

Regarding the temporal series, the combined effects of Events 8 and 9 are shown to reproduce the actual shock arrival on 4 April 2001. This SAT is followed by shocks from

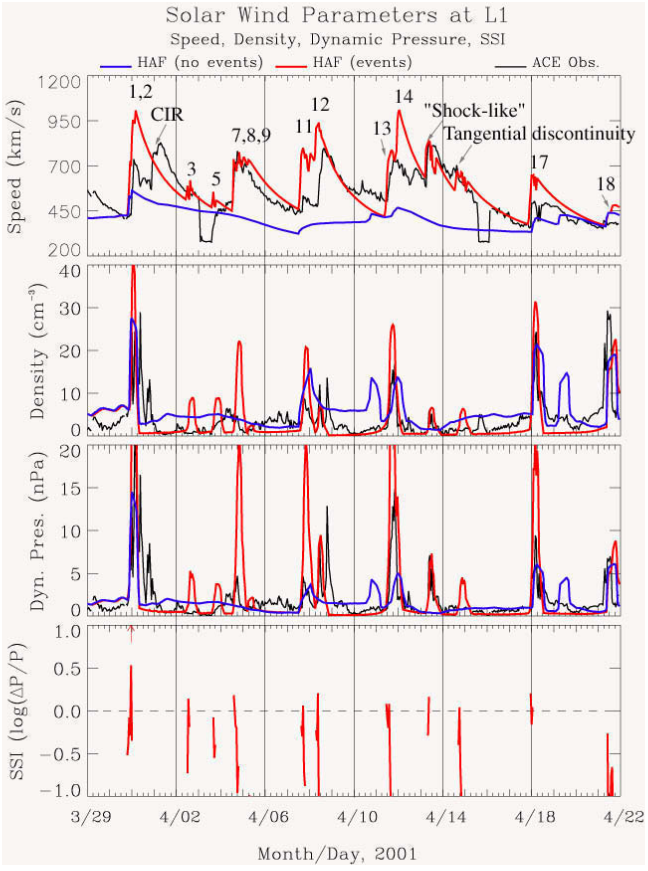

Fig. 7. Comparison of iterated, *ex post facto* time series of simulated (red curves) solar wind speed, density, and dynamic pressure with the actual (black curves) real-time ACE data at LI during the "April Fool's Day" epoch. The relative factors by which the individual V_s values were changed are given in Table 2.

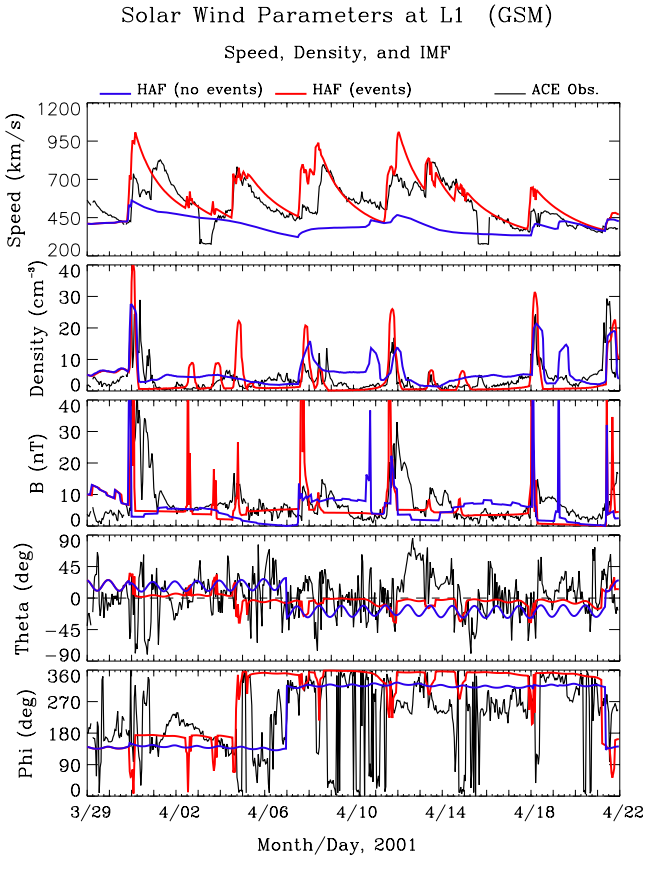

Fig. 8. Iterated, *ex post facto* time series of simulated solar wind plasma and magnetic field parameters at L1 and their comparison with the actual ACE real-time data, as in Fig. 7. The speed and density are repeated from Fig. 7. B is the total IMF magnitude; theta (θ) is the IMF's polar angle in GSM coordinate system and phi (ϕ) is the IMF's azimuthal angle in GSE coordinate system. The color code for the three curves is identical to that used in Fig. 7.

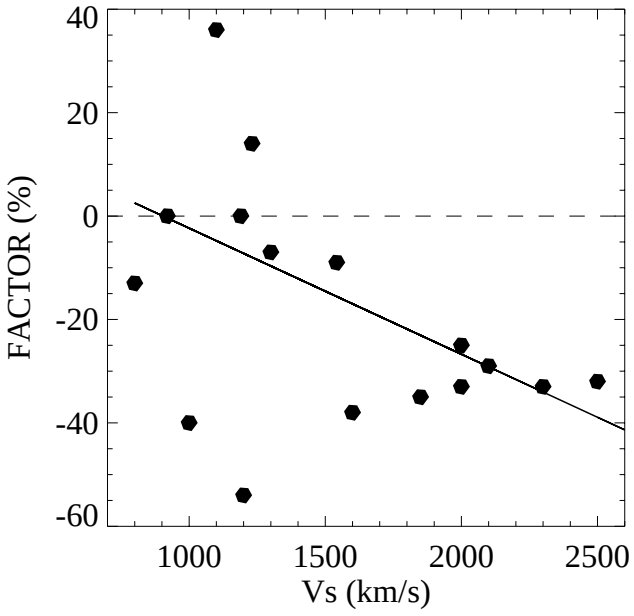

Fig. 9. Distribution of the *ex post facto* coronal shock speed corrective factors, where the factor = $(V_{si} - V_s)/V_s$, in terms of the reported, real-time value V_s used.

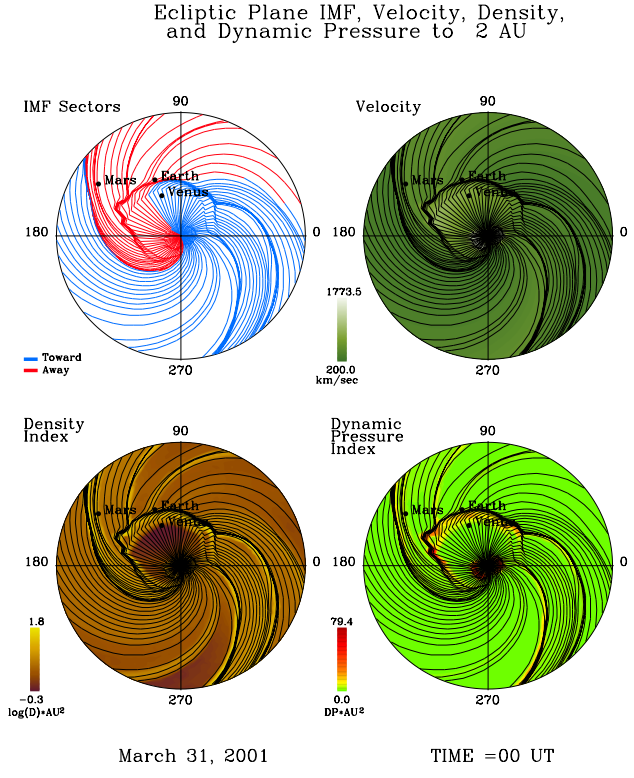

Fig. 10. Ecliptic plane plots (out to 2 AU) of the shock parameters from Event 2 (Table 1) at the time of impending Earth impact that was followed by the monster geomagnetic storm (see Fig. 2). From upper left to lower right, these plots show the IMF distortions, the solar wind speed, solar wind density, and dynamic pressure.

Events 11 and 12 on 7 and 8 April. The shock-like and tangential discontinuity (Table 1) arrivals on, respectively, 13 and 14 April are also shown. The shock from Event 16 ("Gagarin" flare, so named after the Soviet cosmonaut to commemorate the date of the first human flight in space) decayed within the fast stream, thereby producing the tangential discontinuity. Finally, the shocks from the "Easter" X14.4 flare and the subsequent W120° flare (61 h later, from the same AR 9415) are shown, respectively, at ∼00:00 UT, 18 April, and ∼15:00 UT, 21 April 2001, thereby bringing our "April Fool's Day" epoch to an interesting close.

Figure 9 shows the distribution of this iterated "forecast" result, listed in Table 2, in terms of the real-time reported metric Type II shock speed, V_s. The least-squares fitted line shows a tendency of the corrective factor toward low negative values when V_s is very high. This result suggests that the reported initial speed of coronal shock waves must be substantially reduced (30% on average) for most high speed reports. Note, however, that the points in Fig. 9 are quite scattered when V_s is lower than ∼13:00 km/sec.

We return to the ICME shock that arrived at the beginning of the epoch, due to the X1.7/1N flare (Event 2) that arrived (Table 1) at 00:21 UT on 31 March and which initiated the massive geomagnetic storm. Figure 10 shows four plots for the global distorted IMF, solar wind speed, dynamic pressure, and solar wind density within the ecliptic plane, as well as the portion of the simulated shock as it was about to impact the Earth's magnetosphere. The post-shock parameters could be inferred from viewing the sunward values, including the high speeds, temporarily enhanced dynamic pressure, and extremely low densities characteristic of the over expansion of original shock-compressed plasma. Not shown in the distorted IMF are the draped field lines that have been suggested by scenarios that include flux rope diagrams within the ICME.

6 Concluding remarks

We chose a period starting from 28 March 2001 when a central meridian solar flare took place, thereby initiating an intense period of solar and geomagnetic activity during the declining phase of Solar Cycle 23. We ended this period, called the "April Fool's Day" Epoch on 21 April 2001 when a "hemisphere busting" interplanetary shock arrived at Earth after its production by a flare at W120°. This period is of particular interest, not just from its activity, but also because our group made real-time predictions of the shock arrival at L1. Eight of the eighteen solar events produced fast mode forward shocks that were detected by ACE/SWEPAM/MAG real-time data; one event produced a slow mode shock; and eight events produced no L1-detected shocks. The latter negative cases were directed away from Earth either due to their weaker far-eastern or far-western solar sources (flare or helmet-streamer disruption).

The HAFv.2 modeled correctly the eight fast mode forward ICME shocks as distributed in real-time to a wide group

of interested scientists and operational forecasters. However, the ΔT's were on the order of 10–12 h, as determined by a cursory inspection of the time series of predicted and actual observations (Fig. 4). Thus, we modified the most important initialization parameter: the coronal shock speed in an *ex post facto* exercise to improve the ΔTs (Fig. 7) via a simple iterative procedure. We found that this procedure generated an error bar of $\pm 30\%$ in the accuracy of the real-time reported metric Type II coronal shock wave speeds. This parameter, given the location of the solar flare and duration of the still undefined energy release process, is the most important physically significant characteristic of the process that will determine the accuracy of the shock arrival at L1 though non-uniform upstream conditions. Therefore, we recommend development of an operational, 3D coronal density model that would be appropriate for application to specific flares and their metric Type II radio bursts.

Acknowledgements. This work was performed with the support of the DoD University Partnering for Operational Support (UPOS) project, Geoeffectiveness of Solar Events, A83-05. One of the authors (MD) also acknowledges the hospitality of NOAA's Space Environment Center. Also, MAK and KGG acknowledge support of Grant No. MUI05/98 from the Bulgarian Science Fund. The authors thank Dr. Daniel Berdichevsky of NASA's ISTP/SPOF program for unselfishly sharing his preliminary shock identifications. We are also grateful to the NASA/ACE team for providing real-time solar wind data at L1. We also thank Drs. Gareth Lawrence and Kevin Schenk for their near real-time communications of SOHO/LASCO/EIT coronal mass ejections.

The Editor in Chief thanks R. Hunsucker and S. Poedts for their help in evaluating this paper.

References

Chapman, S. and Ferraro, V. C. A.: A new theory of magnetic storm, Part I: Initial phase, Terr. Mag. Atmosph. Elect., 36, 77, 1931.

Dryer, M.: Interplanetary studies: Propagation of disturbances between the Sun and the magnetosphere, Space Sci. Rev., 67 (3/4), 363–419, 1994.

Dryer, M., Fry, C. D., Sun, W., Deehr, C. S., Smith, Z., Akasofu, S.-I., and Andrews, M. D.: Prediction in real-time of the 2000 July 14 heliospheric shook wave and its companions during the "Bastille" Epoch, Solar Phys., in press, 2002.

Fry, C. D., Sun, W., Deehr, C. S., Dryer, M., Smith, Z., Akasofu, S.-I., Tokumaru, M., and Kojima, M.: Improvements to the HAF solar wind model for space weather predictions, J. Geophys. Res., 106, 20 985–21 001, 2001.

Gonzalez, W. D., Joselyn, J. A., Kamide, Y., Kroehl, H. W., Rostoker, G., Tsurutani, B. T., and Vasyliunas, V. M.: What is a geomagnetic storm?, J. Geophys. Res., 99, 5771–5792, 1994.

Kartalev, M. D., Grigorov, K. G., Smith, Z., Dryer, M., Fry, C. D., Sun, W., and Deehr, C. S.: Comparative study of predicted and experimentally detected interplanetary shocks, in: Proceedings of EuroConference on Solar Cycle and space weather, Vico Equense, Italy, 24–29 September 2001, ESA Publ., 477, in press, 2002.

Smith, Z., Dryer, M., Ort, E., and Murtagh, W.: Performance of interplanetary shock propagation models: STOA and ISPM, J. Atm. Solar-Terr. Phys., 62, 1265–1274, 2000.